Geotechnical Aspects of Underground Construction in Soft Ground – Yoo, Park, Kim & Ban (Eds)
© 2014 Korean Geotechnical Society, Seoul, Korea, ISBN 978-1-138-02700-8

Settlements of buildings and buried pipelines induced by adjacent deep excavation in Shanghai soft ground

Y.P. Dong, H.J. Burd & G.T. Houlsby
University of Oxford, Oxford, UK

ABSTRACT: The excavation-induced ground movement may cause deformation to adjacent infrastructure, e.g. buildings, and buried pipelines, which can be investigated through finite element analysis. The purpose of this paper is to investigate settlements of buildings and buried pipelines induced by adjacent deep excavation based on a case study through advanced finite element analysis, which incorporates both the excavation and adjacent buildings and buried pipelines. A multiple-yield surface model is adopted to represent the small-strain stiffness of the soil, with parameters derived from laboratory experiments and in-situ tests. Several important features are considered, e.g. small-stain stiffness of the soil, the construction joints in the diaphragm wall, thermal effects in the concrete slabs, and cracking of the concrete. This research provides information on the appropriate numerical procedures for the prediction of deformations in the nearby infrastructure induced by deep excavations.

1 INTRODUCTION

The excavation induced ground movements may cause deformation and damage in the adjacent infrastructure such as buildings and buried pipelines. The interaction between buildings and deep excavations is particularly complicated, and depends on a many factors, e.g. properties of the soil and structures, building type and configuration, foundations, the distance and relative position of buildings to the excavation, and the excavation activities. Finite element analysis is an effective way to investigate this problem, but detailed analysis has rarely seen in publications, probably due to the complexity.

Most previous studies in this topic, both simplified 2D or detailed 3D analyses (Lee et al., 2011, Dong et al., 2013a, Dong et al., 2013b), are concerned with the excavation behavior in the absence of adjacent infrastructure. The analysis in this paper, however, presents a detailed case study of a deep excavation case history, basement excavation for Shanghai Xingye Bank building, incorporating both the deep excavation and adjacent infrastructure.

The purpose of this study is mainly to demonstrate an appropriate way to consider adjacent infrastructure in the 3D model and evaluate its capability to reproduce the observed behavior in the field. Other aspects, e.g. the influence of several factors on this complex soil-structure interaction problem, and the governing parameters on the settlement of buildings, are beyond the scope of this paper, and will appear on other publications of the authors.

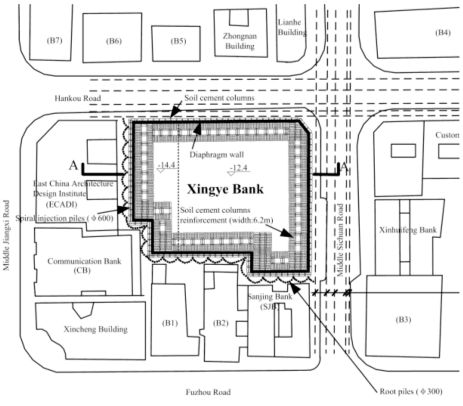

Figure 1. Plane view of the deep excavation (Xu, 2007).

2 CASE HISTORY DESCRIPTION

2.1 *General description*

Shanghai Xingye Bank building is a high-rise building (82.5 m high) with a three-level basement, constructed from a reinforced concrete frame (Wang and Wang, 2007, Xu, 2007). The basement excavation is about 80 m × 90 m in plane, as shown in Figure 1, 14.2 m deep on the west side, and 12.2 m deep on the east side. The excavation is surrounded by 15 densely packed buildings and several old pipelines.

The A-A sectional view (see Figure 1) of the excavation in Figure 2 shows briefly the structure of the retaining system which is mainly composed of the

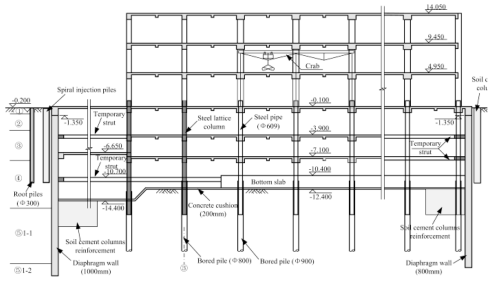

Figure 2. A-A section view (Xu, 2007).

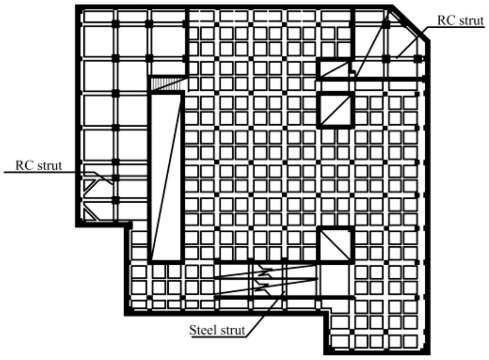

Figure 3. Roof beams and floor slabs (Xu, 2007).

diaphragm wall, horizontal beams and floor slabs, and vertical piles and columns. The diaphragm wall varies from 25.2 m to 31.2 m deep, between 0.8 m and 1.0 m thick. The columns of the main structure are firmly connected with the underneath bored piles. There are mainly 3 levels of permanent floor slabs, one level of temporary strut, and one bottom slab. The superstructure was constructed to the third floor at the end of the basement excavation.

The horizontal support system, as shown in 2.2, is mainly composed of cast-in-situ reinforced concrete beams, floor slabs, and temporary struts.

2.2 *Information on adjacent buildings and pipelines*

There are mainly 15 adjacent buildings (eight historic buildings, including some masonry structures), but only 3 of them are focused in this study, i.e. the ECADI building, the CB building, and the SJB building. The pipelines focused are two electric power pipelines on the east and north sides, which are closest to the excavation (about 3 m to the diaphragm wall), buried 1.3 m below the ground level.

The ECADI (East China Architecture and Design Institute) building is situated about 4.8 m on the west side of the excavation. The main building, originally built in 1949, has an 8-story (37.2 m high) reinforced concrete frame structure, supported on a reinforced concrete box foundation with timber piles. The CB (Communication Bank) building is situated around 4.8 m on the South West side of the excavation. The

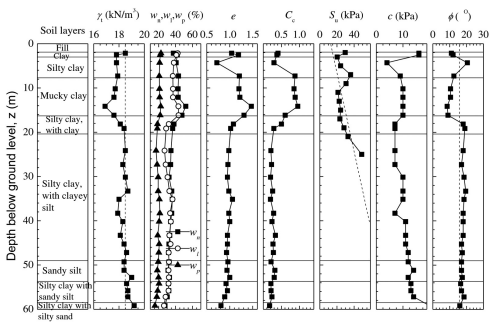

Figure 4. Geotechnical profile and soil properties (Xu, 2007).

building, built in 1927, has a reinforced concrete frame structure (25.9 m) founded on a slab-and-beam type raft foundation with timber piles. The SJB (San Jing Bank) building is situated approximately 4.0 m on the South side of the excavation. The building, built in 1934, has a 5-storey brick and wood structure (around 20 m high), founded on a strip footing.

2.3 *Geotechnical conditions*

According to site investigation report (SGIDI, 1997), the site is on a flat coastal plain, with ground elevation between 4.80 m to 3.87 m. The ground water table is 0.5 m to 1 m below the ground surface. The site is underlain by thick, relatively soft quaternary alluvial and marine deposits. The geological profile and soil properties from site investigation of this project are shown in Figure 4. The natural water content of clay and silty clay layer is close to, or higher than, the liquid limit, suggesting that the soil is either normally consolidated or lightly overconsolidated. The undrained shear strength s_u, determined from field vane shear test, is significantly higher than the value normally associated with clay at the liquid limit, indicating that the soft clay is likely to be sensitive. The permeability of the soft layers clay is in the order of 10^{-9} m/s, indicating that the clay is close to the undrained condition during the excavation. The average unit weight $\gamma = 18.50\,\text{kN/m}^3$, and friction angle $\varphi = 15°$, are adopted for convenience.

The soil properties shown in Figure 4 are not sufficient to derive all the input parameters for the advanced soil model in the analysis, e.g. the small-strain stiffness nonlinearity of the soil. Therefore, additional data are collected from publications on Shanghai clay.

2.4 *Construction sequence*

The construction followed a typical top-down method. The major construction sequences are summarized in Table 1.

2.5 *Field instrumentation*

The detailed layout of instrumentation is shown in Figure 5. The measured items mainly include wall deformations, ground movements, settlement of adjacent buildings and pipelines, and pore water pressures.

Table 1. Construction sequences.

Stages	Construction activities
1	Install diaphragm walls and bored piles; conduct ground improvement and dewatering;
2	Excavate to −1.5 m, then to −5.3 m with earth berms;
3	Cast the roof beams and floor slabs of the basement;
4	Excavate the earth berms to −5.3 m;
5	Cast the – 1st beams and floor slabs of the base ment, and the ground floor of the superstructure;
6	Excavate to −8.55 m;
7	Cast beams and slabs for the – 2nd floor of the basement, and the first floor of the superstructure;
8	Excavate to −10.7 m first, then to −12.4 m with earth berms; remove the earth berms to −11.3 m;
9	Cast the bottom slab and temporary struts for the – 3rd floor of the basement, and the 2nd floor of the superstructure;
10	Excavate the remaining soil to −14.4 m (west side) and −12.4 m (east side) respectively; cast the concrete cushion;
11	Cast the bottom slab on the west side; remove the temporary struts; construct the remaining structures.

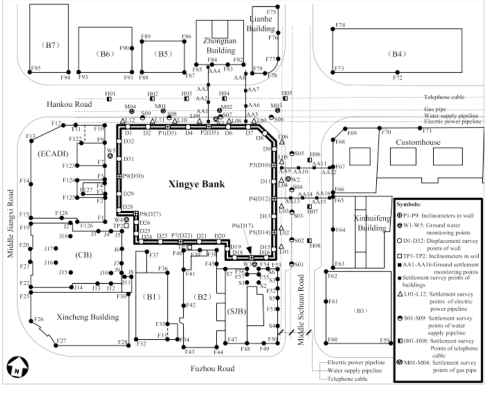

Figure 5. Field instrumentation (Xu, 2007).

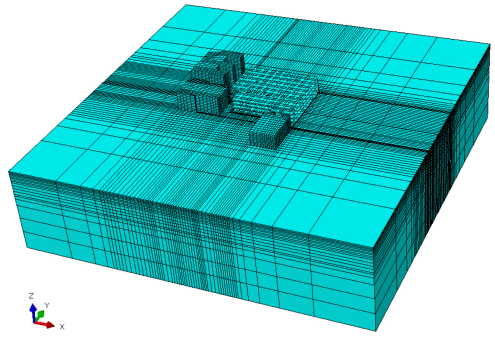

Figure 6. Mesh for the whole model (400 m × 400 m × 100 m).

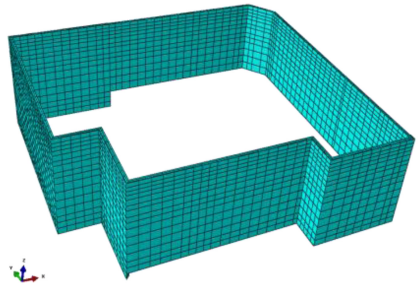

Figure 7. Mesh for the diaphragm wall.

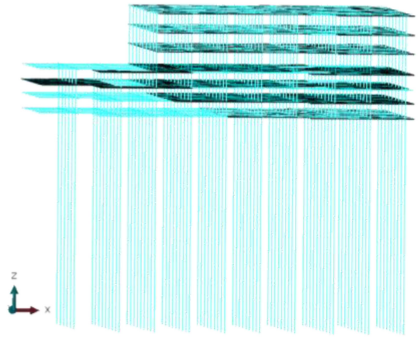

Figure 8. Mesh for the retaining system.

3 FINITE ELEMENT MODEL DESCRIPTION

3.1 *Mesh and geometry*

The mesh of the whole finite element model, developed in ABAQUS 6.11, is shown in Figure 6. This model incorporates the detailed retaining structure (the diaphragm wall, horizontal beams and floor slabs, vertical piles and columns), adjacent buildings and buried pipelines, and the ground improvement, and considered actual construction sequences. The model size is 400 m × 400 m × 100 m, and the boundary is sufficiently remote from excavation edge. Four vertical boundaries are rollers, and the bottom is fixed. The model has a total of 102036 elements and 116756 nodes.

The soil is modelled with 8-noded solid hexahedral elements with reduced integration (C3D8R).

The mesh for the diaphragm wall is shown in Figure 7. Solid elements (C3D8R) are used to model the diaphragm wall.

The support system, as shown in Figure 8, includes vertical piles and columns, horizontal beams, floor slabs, and the superstructure constructed during the excavation. The piles and beams are modelled with 3D 2-noded beam elements (B31), while the floor slabs are modelled with 4-noded quadrilateral shell elements with reduced integration (S4R).

The geometry and structure of buildings are simplified to reduce the complexity. The external walls (0.3 m thick), internal walls (0.2 m thick), and floors (0.15 m thick) of buildings, are modelled using shell

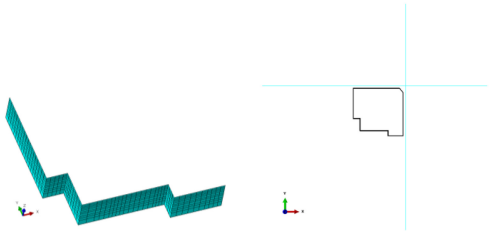

Figure 9. Mesh for the ground improvement and pipelines.

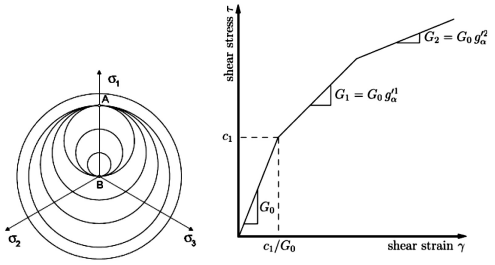

Figure 10. Multiple-yield surface soil model (Houlsby, 1999).

elements (S4R). Openings in the walls and floors are not considered in the model for simplicity. Foundations of buildings are assumed due to limited known information. The raft foundations (1.3 m thick) are modelled using solid elements (C3D8R). Timber piles (Φ300 mm) are modelled with beam elements (B31). The ground improvement (0.3 m thick) and buried pipelines (Φ500 mm, wall thickness 20 mm), as shown in Figure 9, are modelled by shell elements (S4R) and beam elements (B31) respectively.

3.2 *Material models and input parameters*

3.2.1 *Soil model and input parameters*

The soil is represented by a multiple-yield surface model (Houlsby, 1999), as shown in Figure 10, to consider the small-strain stiffness nonlinearity of the soil, using soil properties derived for Shanghai soft clay. This soil model uses multiple yield surfaces within the framework of work-hardening plasticity theory. Nonlinearity of the small-strain response is achieved using a number of nested yield surfaces of the same shape as the outer fixed failure surface. As a stress point moves in the stress space and encounters a yield surface, the stiffness reduces, and the yield surface moves with the stress point. This soil model was used in the tunneling installation (Burd et al., 2000) and has been implemented into ABAQUS through the subroutine UMAT for deep excavations (Dong et al., 2013a, Dong et al., 2013b).

The undrained shear strength s_u, as shown in Equation (1) increases linearly with depth z.

$$s_u = (20 + 2z)kPa \tag{1}$$

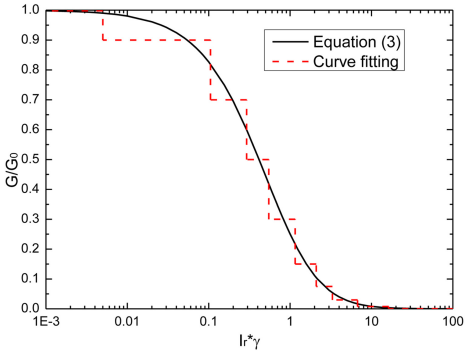

Figure 11. Curve fitting for parameters of multi-surface model.

The shear stiffness at very small strain G_0, as shown in Equation (2), is related to the undrained shear strength s_u through the index of rigidity I_r.

$$G_0 / s_u = I_r = 1000 \tag{2}$$

Other parameters include bulk modulus $K = 50G_0$ in undrained condition, the coefficient of lateral earth pressure $K_0 = 0.74$, and the unit weight $\gamma = 18.50\,\text{kN/m}^3$. The relationship between the tangent shear stiffness G_t and shear strain γ, as shown in Equation (3), is derived from laboratory test data published about Shanghai clay.

$$\frac{G_t}{G_0} = \frac{1}{\left(1 + I_r \cdot \gamma\right)^2} \tag{3}$$

The input parameters for the multi-yield surface soil model are derived from the Equation (3), using the stepwise fitting as shown in Figure 11. The plot of $G_t/G_0 \sim I_r \cdot \gamma$ is found to be more useful because G_t/G_0 is independent of the specific value of I_r.

3.2.2 *Material model for structures*

The structural components are mainly reinforced concrete structures.

The diaphragm wall is modelled with anisotropic elastic properties to consider joints in the wall (Zdravkovic et al., 2005). The elastic properties of concrete are $E = 30\,\text{GPa}$, $\nu = 0.2$. The out-of-plane stiffness E_{out} is reduced compared to its in-plane stiffness ratio E_{in} by a factor of $E_{\text{out}}/E_{\text{in}} = 0.1$, based on back analyses of this case history.

Horizontal beams and floor slabs are modelled as a linear elastic material including thermal shrinkage of concrete due to temperature change during curing process and ambient temperature variation (Whittle et al., 1993, Hashash et al., 2003, Boone and Crawford, 2000). The Coefficient of Thermal Expansion (CTE) is $1 \times 10^{-5}/°\text{C}$, associated with temperature change $\Delta T = -35°\text{C}$ which is also based on back analysis.

The buildings are represented by a linear elastic material, with unit weight $\gamma = 10\,\text{kN/m}^3$, and stiffness $E = 20\,\text{GPa}$, $\nu = 0.2$, to consider openings and

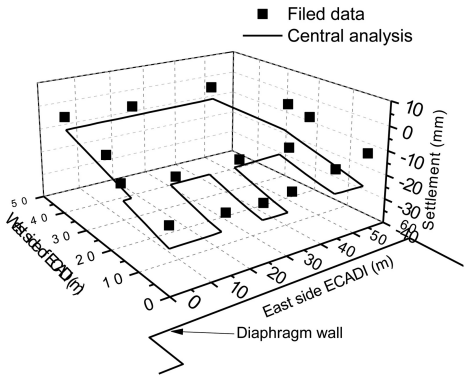

Figure 12. Settlement of ECADI building.

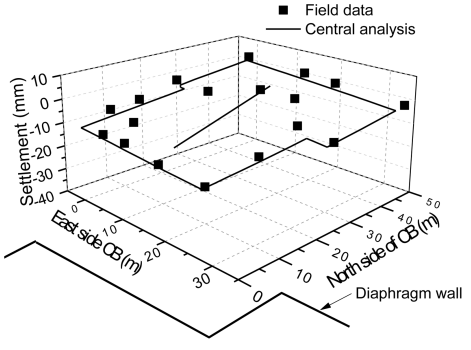

Figure 13. Settlement of CB building.

cracks in buildings. The raft foundations and pipelines are assumed to be linear elastic, $E = 20$ GPa, $\nu = 0.2$. The ground improvement is anisotropic linear elastic to consider the discontinuities between adjacent piles, $E = 3$ GPa, $\nu = 0.2$, $E_{out}/E_{in} = 10^{-5}$.

4 NUMERICAL ANALYSIS AND RESULTS

4.1 *Building settlements*

The computed settlements of these 3 buildings along the building outlines at the final stage of the excavation, are compared with the field measurement in Figure 12 to Figure 14.

The results indicate that all three buildings deform in a rigid manner and tilt towards the excavation, probably due to the high stiffness of the buildings and foundations used in the analysis. The computed settlements generally agree well with, but are slightly larger than, the field measurement, especially the ECADI building. The discrepancy might be attributed to a number of factors, e.g. the soil properties, the structural details and properties, the type of the foundations, the construction activities, and the reliability of the field measurement. For example, the internal structures and foundations of these buildings are assumed; the stiffness and weight of the buildings are estimated; the soil underneath those buildings might be stiffer

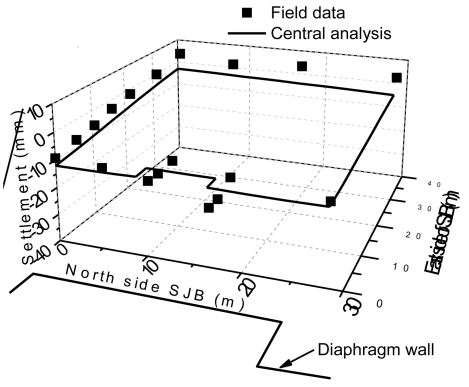

Figure 14. Settlement of SJB building.

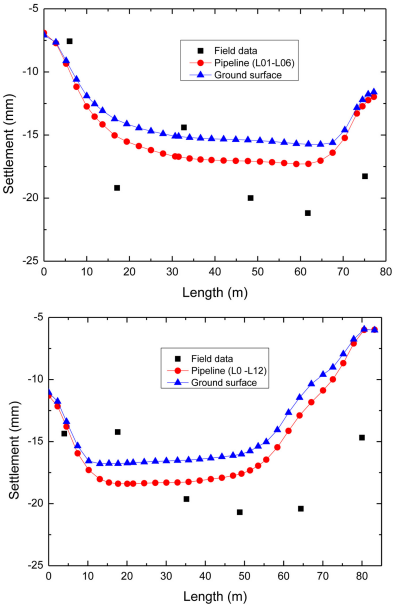

Figure 15. Settlements of pipelines and above ground surface.

and stronger than the soil in the greenfield site, which is not considered in the soil model. It is difficult to consider all these aspects appropriately in the numerical modelling due to the limitations of computational capabilities and uncertainties in determining material properties.

4.2 *Settlements of buried pipelines*

The computed settlements of buried pipelines from the final stage of the excavation are compared with the field measurement in Figure 15. The ground surface settlements above the buried pipelines are also shown in the figure, because they are commonly used to represent the settlements of the buried pipelines in the field measurement.

The calculated settlements of two pipelines agree well with the field measurement in pattern, but are

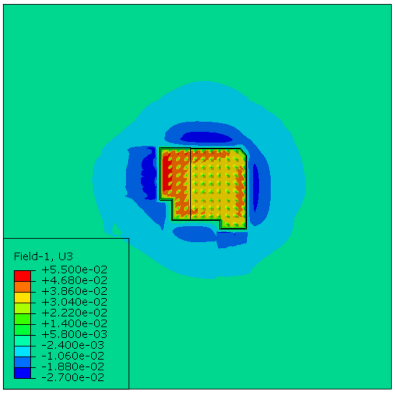

Figure 16. Contour of vertical ground movement (unit: m).

slightly smaller in magnitude. It is also found that the ground surface settlements over the pipelines are slightly smaller than the pipeline settlements, but with a similar pattern, probably due to the swelling of the soil in the retained area of the excavation. If the small difference is neglected, the results suggest that it is reasonable in practice to use the ground surface settlement to represent the settlement of buried pipelines, and in the numerical analysis the pipelines might not be necessary to include in the model.

4.3 *Contour of vertical ground movement*

It is seen from the plan view of the vertical ground movement in Figure 16 that the ground settlements outside the excavation are concentrated in the small areas behind the diaphragm wall and vanish far away from the edge of the excavation. The settlement is smaller around the wall corner due to the corner effect. When comparing the ground settlement patterns in the areas with and without buildings, it is found that the ground movement is modified due to the existence of buildings. The basal heave of the soil inside the exaction is larger at the left side because the excavation is deeper in this side, and is larger close to the diaphragm wall probably due to the inward movement of the wall.

5 CONCLUSIONS

This case study focuses on settlements of buildings and buried pipelines induced by adjacent deep excavation. The finite element model developed in this paper incorporates both excavation and adjacent infrastructure such as buildings, buried pipelines, and the ground improvement, representing an analysis more close to the real situation. The computed building settlements agree well with the field measurement, while the small discrepancy might be attributed to assumptions made in the analysis and uncertainties in determining the input parameters. The computed settlements of pipelines also agree well with the field measurement, but are slightly larger than the above ground settlements probably due the swelling of the soil. This indicates that it is suitable to measure the ground surface settlement to represent the settlement of buried pipelines. The influence of several important aspects on the settlement of buildings (e.g. stiffness, weight, foundation, and ground improvement) and pipelines (e.g. diameter, wall thickness, stiffness, and element types), will be discussed in other publications of the authors.

ACKNOWLEDGEMENT

The field data was collected and analyzed by Dr Zhonghua Xu, a PhD graduate of Shanghai Jiao Tong University in his PhD thesis. The calculations were conducted on Oxford supercomputer.

REFERENCES

Boone, S. J. & Crawford, A. M. 2000 Braced excavations: Temperature, elastic modulus, and strut loads. Journal of Geotechnical and Geoenvironmental Engineering, 126, 870–881.

Burd, H. J., Houlsby, G. T., Augarde, C. E. & Liu, G. 2000 Modelling tunnelling-induced settlement of masonry buildings. Proceedings of the Institution of Civil Engineers: Geotechnical Engineering, 143, 17–29.

Dong, Y. P., Burd, H. J., Houlsby, G. T. & Hou, Y. M. (2013a) Advanced Numerical Modelling of a Complex Deep Excavation Case History in Shanghai. 5th International Young Geotechnical Engineers' Conference. Paris.

Dong, Y. P., Burd, H. J., Houlsby, G. T. & Xu, Z. H. (2013b) 3D FEM Modelling of a Deep Excavation Case History Considering Small-strain Stiffness of Soil and Thermal Shrinkage of Concrete. 7th International Conference on Case Histories in Geotechnical Engineering. Chicago.

Hashash, Y. M. A., Marulanda, C., Kershaw, K. A., Cording, E. J., Druss, D. L., Bobrow, D. J. & Das, P. K. 2003 Temperature correction and strut loads in Central Artery excavations. Journal of Geotechnical and Geoenvironmental Engineering, 129, 495–505.

Houlsby, G. T. (1999) A model for the variable stiffness of undrained clay. Proceedings of the International Symposium on Pre-Failure Deformations of Soil. Torino.

Lee, F., Hong, S., Gu, Q. & Zhao, P. 2011 Application of Large Three-Dimensional Finite-Element Analyses to Practical Problems. International Journal of Geomechanics, 11, 529–539.

SGIDI (1997) Geotechnical site investigation report of Shanghai Xingye Bank Building. Shanghai, Shanghai Geotechnical Investigations & Design Institute Co. Ltd.

Wang, W. D. & Wang, J. H. (2007) Design, analysis and case histories of deep excavations supported by permanent structures, Beijing, China Architecture & Building Press.

Whittle, A. J., Hashash, Y. M. A. & Whitman, R. V. 1993 Analysis of deep excavation in Boston. Journal of Geotechnical Engineering – ASCE, 119, 69–90.

Xu, Z. H. (2007) Deformation Behaviour of Deep Excavations supported by Permanent Structure in Shanghai Soft Deposit. Department of Civil Engineering. Shanghai, Shanghai Jiao Tong University, China.

Zdravkovic, L., Potts, D. M. & St. John, H. D. 2005 Modelling of a 3D excavation in finite element analysis. Geotechnique, 55, 497–513.